Simulation of non-Gaussian stochastic processes by amplitude modulation and phase reconstruction

Yu Jiang[*1], Junyong Tao[1a] and Dezhi Wang[2b]

[1]*Laboratory of Science and Technology on Integrated Logistics Support, College of Mechatronic Engineering & Automation, National University of Defense Technology, Changsha 410073, China*
[2]*Centre for Engineering Dynamics, University of Liverpool, Liverpool, UK*

Abstract. Stochastic processes are used to represent phenomena in many diverse fields. Numerical simulation method is widely applied for the solution to stochastic problems of complex structures when alternative analytical methods are not applicable. In some practical applications the stochastic processes show non-Gaussian properties. When the stochastic processes deviate significantly from Gaussian, techniques for their accurate simulation must be available. The various existing simulation methods of non-Gaussian stochastic processes generally can only simulate super-Gaussian stochastic processes with the high-peak characteristics. And these methodologies are usually complicated and time consuming, not sufficiently intuitive. By revealing the inherent coupling effect of the phase and amplitude part of discrete Fourier representation of random time series on the non-Gaussian features (such as skewness and kurtosis) through theoretical analysis and simulation experiments, this paper presents a novel approach for the simulation of non-Gaussian stochastic processes with the prescribed amplitude probability density function (PDF) and power spectral density (PSD) by amplitude modulation and phase reconstruction. As compared to previous spectral representation method using phase modulation to obtain a non-Gaussian amplitude distribution, this non-Gaussian phase reconstruction strategy is more straightforward and efficient, capable of simulating both super-Gaussian and sub-Gaussian stochastic processes. Another attractive feature of the method is that the whole process can be implemented efficiently using the Fast Fourier Transform. Cases studies demonstrate the efficiency and accuracy of the proposed algorithm.

Keywords: stochastic simulation; non-Gaussian; amplitude modulation; phase reconstruction

1. Introduction

Engineering structures are often subjected to stochastic loadings such as earthquakes, winds or ocean waves. Most loadings in nature can be modeled as Gaussian processes in light of the central limit theorem. However, the stochastic processes show non-Gaussian properties in some practical applications, such as the random vibrations generated by wheeled vehicles travelling over irregular terrain, and wind pressure fluctuations on building envelopes. Numerical simulation method is

---

∗Corresponding author, Associate professor, E-mail: jiangyu@nudt.edu.cn
[a] Professor, E-mail: taojunyong@gmail.com
[b] Ph. D. student, E-mail: wang_dezhi@hotmail.com

widely applied for the solution to stochastic problems of complex structures when alternative analytical methods are not applicable. When the stochastic processes deviate significantly from Gaussian, techniques for their accurate simulation must be available.

The simulation of Gaussian processes has been explored for several decades, while non-Gaussian simulation has not been as widely addressed. Yamazaki and Shinozuka (1988) proposed a method of simulating non-Gaussian time series by a nonlinear static transformation from Gaussian to non-Gaussian with the aid of an iterative procedure. Spectral Correction method based on modified Hermite polynomial transformation for the simulation of a class of non-normal random processes has been presented by (Gurley 1996). Seong and Peterka (1998) presented a new method based on the Fourier representation of random time series for generating artificial surface-pressure time series focused on the simulation of non-Gaussian spiky fluctuation features. Suresh Kumar and Stathopoulos (1999) presented an efficient and practical method based on the Fast Fourier Transform (FFT) for the digital generation of univariate non-Gaussian wind pressure time series on low building roofs. Gioffrè *et al*. (2000) proposed a simulation algorithm using the correlation-distortion method based on translation vector processes to generate non-Gaussian wind pressure fields. Choi and Kanda (2003) reviewed several simulation methods based on the translation method using logarithmic and polynomial functions for simulating the non-Gaussian stationary process. Phoon and Huang (2005) proposed a simulation algorithm using Karhunen-Loeve expansion to generate strongly non-Gaussian processes. Yu (2008) presented an algorithm for generating super-Gaussian random loadings by the Fast Fourier Transform (FFT) and second phase modulation (SPM). Bocchini and Deodatis (2008) reviewed and introduced the latest developments of a class of simulation algorithms for strongly non-Gaussian random fields. Poirion and Puig (2010) presented a simulation technique of multivariate non-Gaussian random processes and fields based on Rosenblatt's transformation of Gaussian processes. Shields and Deodatis (2011) presented a technique for simulation of strongly non-Gaussian stochastic vector processes using translation process theory. Zentner *et al*. (2011) presented a new method for generating synthetic ground motion based on Karhunen-Loeve decomposition and a non-Gaussian stochastic model. Aung and Ye (2011) presented a stochastic non-Gaussian simulation algorithm using a cumulative distribution function (CDF) mapping technique that converges to a desired target power spectral density. Yura and Hanson (2012) proposed a simulation method of two-dimensional random fields with arbitrary power spectra and non-Gaussian probability distribution functions. The method relies on initially transforming a white noise sample set of random Gaussian distributed numbers into a corresponding set with the desired spectral distribution, after which this colored Gaussian probability distribution is transformed via an inverse transform into the desired probability distribution. Li and Li (2012) presented a direct simulation algorithm by expanding the autoregressive (AR) model and the autoregressive moving average (ARMA) model for the generation of a class of non-Gaussian stochastic processes according to target lower-order moments and prescribed power spectral density (PSD) function. Ye and Liu (2012) presented a simplified simulation method of non-Gaussian wind load based on the inverse fast Fourier transform (IFFT), in which the amplitude spectrum is established via a target power spectrum and the phase spectrum is constructed by introducing the exponential peak generation (EPG) model. Luo *et al*. (2012) presented a simulation methodology of the stationary non-Gaussian stochastic wind pressure field based on the zero memory nonlinearity translation method and the spectral representation method. Li and Wang (2012) presented an exponential model for fast simulation of multivariate non-Gaussian processes with application to structural wind engineering. Vargas-Guzmán (2012) presented new parametric heavy-tailed distributions for

non-Gaussian simulations with higher-order cumulant parameters predicted from sample data. Aung and Jihong (2012) developed a new wavelet-based CDF mapping technique for simulation of multivariate non- Gaussian wind pressure process. Shields and Deodatis (2013) presented a simple and efficient methodology to approximate a general non-Gaussian stationary stochastic vector process by a translation process.

As mentioned above, there is a wide range of different methodologies in the literature for simulation of non-Gaussian stochastic processes. In general, these previous methods can be broadly classified into three categories as follows: 1) ARMA class model with non-Gaussian white noise, 2) translation process-based, or nonlinear static transformation (NST), from the Gaussian random processes to non-Gaussian processes and 3) the spectral representation method. For category 1, the ARMA approach is based on the simple and well-known theory of linear difference equations and is computationally efficient. However, ARMA models cannot represent data exhibiting sudden spikes of very large amplitude at irregular intervals and having negligible probability of very high level crossings; therefore, these are not suitable for representing strong non-Gaussian time series. For category 2, the basic feature of translation process-based method is to generate a non-Gaussian translation field by mapping an underlying Gaussian process to the desired non-Gaussian marginal probability distribution function (PDF) according to a prescribed power spectral density (PSD). The translation process-based method usually employs iterative schemes to match both the prescribed non-Gaussian marginal PDF and PSD function. But because the transformation of Gaussian process to non-Gaussian process will change both the PDF and PSD in the same time, it is unable to ensure the compatibility between prescribed non-Gaussian PDF and PSD. The spectral representation method, of category 3, is based on discrete Fourier representation of random time series, which consists of the superposition of sinusoids at discrete frequencies that possess deterministic amplitude and random phase. The spectral representation method calculates the amplitude part of the Fourier coefficient (modulus of sinusoids) by the specified PSD, and approximates the non-Gaussian parameters (such as skewness and kurtosis) of a given amplitude PDF by changing the phase part of the Fourier coefficient (phase angles of sinusoids). Since the phase part is free from the second-order properties of random time series (such as PSD), the spectral representation simulation methodology can ensure the compatibility between prescribed Non-Gaussian PDF and PSD. However, previous spectral representation methods only consider and utilize the impact of the Fourier phase coefficients for non-Gaussian characteristics. Therefore, according to the central limit theorem, changing the randomness of the uniformly distributed random phases at different frequencies will strengthen the fluctuating features such as the sharp spike events of the generated random signal. This means that will increase the kurtosis value of the original Gaussian signal, resulting in super-Gaussian random signal.

So the various existing methods of changing the phase part of the Fourier coefficient according to the non-Gaussian parameters (such as skewness and kurtosis) can only simulate non-Gaussian stochastic processes with the high-peak characteristics, that is super-Gaussian. This can be confirmed by the simulation examples of the papers listed in the references. In some cases, sub-Gaussian stochastic processes with less high peaks will be encountered or be useful for important application. For example, shaker power will be increased by the sub-Gaussian random control with decreased kurtosis for the purpose of less risk of damage to the test item and shaker in modal testing (Steinwolf 2007, 2010). Hence in order to simulate sub-Gaussian random processes, it is necessary to study and analysis the coupling effect of both the Fourier phase and amplitude

coefficients on the non-Gaussian features of simulated random process. We will discuss in detail on this issue through theoretical analysis and simulation experiments in the following sections.

2. Theoretical background

The well known spectral representation is based on a discretized model of the target power spectral density (PSD) function $G^T(f)$ for the desired process. The simulation consists of the superposition of harmonics at discrete frequencies that possess deterministic amplitude and random phase (DARP). A zero mean stationary Gaussian realization can be simulated by DARP as $N \to \infty$

$$x(t) = \sum_{k=0}^{N-1} A_k \cos(2\pi f_k t + \phi_k) \tag{1}$$

where A_k are determined by the target one sided PSD values $G^T(f)$ at the corresponding frequencies f_k

$$A_k = \sqrt{2G^T(f_k)\Delta f} \tag{2}$$

$$\Delta f = f_u / N \tag{3}$$

$$f_k = k\Delta f, \quad k = 0,1,\cdots,N-1 \tag{4}$$

f_u is the upper cutoff frequency beyond which $G^T(f)$ can be considered to be zero. ϕ_k is the kth realizations of a uniformly distributed random phase angles from 0 to 2π or from $-\pi$ to π.

In order to improve simulation efficiency by employing the Fast Fourier Transform (FFT), Eq. (1) can be rewritten as

$$x(n\Delta t) = \text{Re}\left\{ \sum_{k=0}^{M-1} A_k e^{i\phi_k} e^{i2\pi f_k n\Delta t} \right\}, \quad n = 0,1,\cdots,M-1 \tag{5}$$

Where Re{.} represents the real part of the expression enclosed in brace, and M is the number of time intervals of length Δt, which is defined by sampling frequency f_s

$$\Delta t = \frac{1}{f_s} \tag{6}$$

According to sampling theorem, f_s must satisfy

$$f_s \geq 2f_u \tag{7}$$

It is obvious that

$$\Delta f = \frac{f_u}{N} = \frac{f_s}{M} \tag{8}$$

Thus, M and N must satisfy $M \geq 2N$.

Inserting Eq. (4), (6) and (8) into (5) yields a discrete fourier representation of time series

$$x(n\Delta t) = \mathrm{Re}\left\{ \sum_{k=0}^{M-1} A_k e^{i\phi_k} e^{i2\pi nk/M} \right\} = \mathrm{Re}\left\{ \mathrm{IDFT}(C_k) \right\} \tag{9}$$

Where IDFT means Inverse Discrete Fourier Transform, and C_k is

$$C_k = A_k e^{i\phi_k} = A_k(\cos\phi_k + i\sin\phi_k), \ \ k = 0, 1, \cdots, M-1 \tag{10}$$

Note that M is selected to be a power of 2 to use the IFFT algorithm.

The realizations of $x(t)$ obtained using either (1) or (5) follow a Gaussian distribution in the limit as $N \to \infty$ due to the Central Limit Theorem and can be considered approximately Gaussian for most practical applications if N is greater than approximately 100.

Zero mean Gaussian stochastic processes can be adequately described by power spectral density, while for non-Gaussian stochastic processes, higher marginal moments, more precisely the marginal skewness and kurtosis, are additionally used to describe the non-Gaussian features. The kurtosis (K) and skewness (S) value of a stochastic processes X is defined by the expression

$$K = \frac{E\left[X - E(X)\right]^4}{\left\{ E\left[X - E(X)\right]^2 \right\}^2} - 3 \tag{11}$$

$$S = \frac{E\left[X - E(X)\right]^3}{\left\{ E\left[X - E(X)\right]^2 \right\}^{3/2}} \tag{12}$$

It should be noted that the kurtosis defined in the Eq.(11) is a normalized value. Under this definition, the kurtosis value of a Gaussian random signal is 0, which is equivalent to a kurtosis value 3 defined in some other literatures.

Kurtosis (K) is used to describe the tail distribution feature of amplitude probability density function, and skewness (S) is used to describe the asymmetry of amplitude probability density function. In case of symmetrical distributions, kurtosis is the most important coefficient used to find out how much the distribution differs from the normal distribution. It is well known that both skewness and kurtosis of Gaussian stochastic processes are equal to zero, and the stochastic processes with $K > 0$ are said over-Gaussian or super-Gaussian stochastic processes, while stochastic processes with $K < 0$ are said sub-Gaussian stochastic processes.

To simulate non-Gaussian processes with given PSD, skewness and kurtosis values by suitable amplitude modulation and phase reconstruction, the relationships between the target characteristics(PSD, skewness and kurtosis) and the variables in the fourier series model in Eq. (10) (amplitude and phase part) should be considered. Since the PSD does not depend on the phase angles (see Eq. (2)), the variation of phase part does not affect the second order characteristics(variance, PSD) of the time series. On the other hand, an earlier study by shows that

the spikes in the time domain, responsible for non-Gaussian nature, are strongly dependent on the phase part of the fourier transform (Seong and Peterka 2001). In this paper, further analysis showed that the skewness and kurtosis of the simulated random process depend not only on the phase part of the fourier transform, but also on the amplitude part. This paper presents a theoretical background of the method in the appendix and a series of simulation experiments in section 3 to understand the mechanism of phase reconstruction by amplitude modulation, which provides a fundamental framework for the simulation method.

As discussed in the appendix, the kurtosis of the random process $x(t)$ can be expressed as the following form

$$K = \left\{ \sum_{k=0}^{N-1} A_k^2 \right\}^{-2} \left\{ -\frac{3}{2} \sum_{k=0}^{N-1} A_k^4 + 2 \sum_{j=3k} A_j A_k^3 \cos(\phi_j - 3\phi_k) + 6 \sum_{\substack{j=k+2n \\ k \neq n}} A_j A_k A_n^2 \cos(\phi_j - \phi_k - 2\phi_n) + \right.$$

$$6 \sum_{\substack{j+k=2n \\ j<k}} A_j A_k A_n^2 \cos(\phi_j + \phi_k - 2\phi_n) + 12 \sum_{\substack{j+k=n+m \\ j<k,n<m,j<n}} A_j A_k A_n A_m \cos(\phi_j + \phi_k - \phi_n - \phi_m) +$$

$$12 \sum_{\substack{j+k+n=m \\ j<k<n}} A_j A_k A_n A_m \cos(\phi_j + \phi_k + \phi_n - \phi_m) \left. \right\} \qquad (13)$$

A similar expression can also be obtained for skewness

$$S = \left\{ \frac{1}{2} \sum_{k=0}^{N-1} A_k^2 \right\}^{-1.5} \left\{ \frac{3}{4} \sum_{j=2k} A_j A_k^2 \cos(\phi_j - 2\phi_k) + \frac{3}{2} \sum_{j+k=m, j<k} A_j A_k A_m \cos(\phi_m - \phi_j - \phi_k) \right\} \quad (14)$$

Eqs. (13) and (14) clearly show that the kurtosis and skewness value of the simulated random process depend not only on fourier phase angles ϕ_k, but also on fourier amplitudes A_k. From intuition, it is not difficult to imagine that if we choose some fourier amplitudes in the Eq. (19) equal to 0, it will make the kurtosis value decreases from 0, so it is possible to generate a sub-Gaussian random signal. However, it is difficult to establish a quantitative relationship between the non-Gaussian parameters (such as kurtosis and skewness) and the Fourier amplitude and phase coefficients. Next, we will reveal the coupling effect of the amplitudes and phases on the non-Gaussian features by two simulation experiments. Then we will further develop the methodology for simulation of various types of non-Gaussian signals by amplitude modulation and phase reconstruction.

3. Experiments of coupling effect of fourier coefficients on the non-Gaussian features

The simulation experiments were performed by modifying the amplitude and the phase separately, or one part was replaced by another signal. Investigation was made of the variation of the non-Gaussian features of the signal obtained by IFFT of the modified Fourier coefficients.
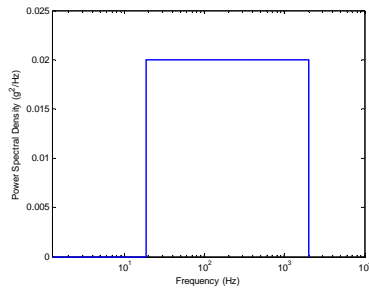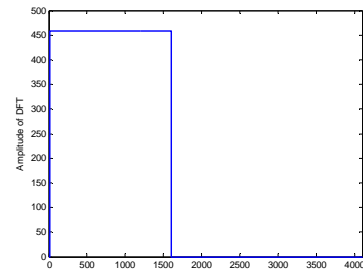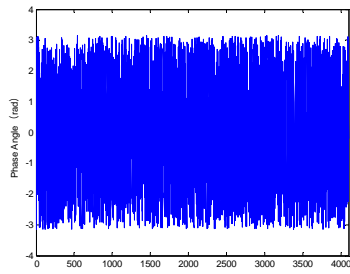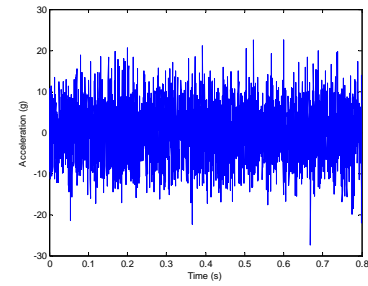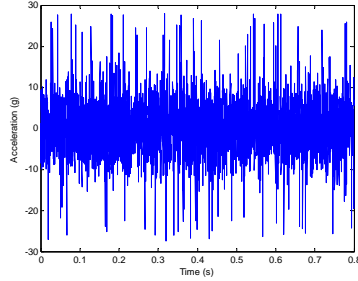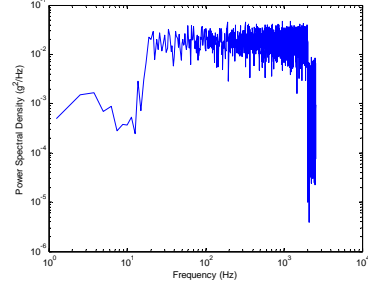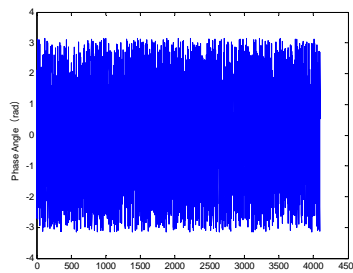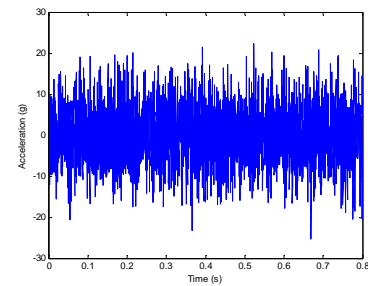
(a) Target PSD $G^T(f)$

(b) Fourier amplitudes $A^T[k]$ of $x_1[n]$

(c) Phase angles $\phi_1[k]$ of $x_1[n]$

(d) Simulated Gaussian signal $x_1[n]$

(e) Modulated signal $x_2[n]$

(f) PSD of $x_2[n]$

(g) Phase angles $\phi_2[k]$ of $x_2[n]$

(h) Simulated signal $x_3[n]$

Fig. 1 Simulation experiment 1

Firstly, according to the target power spectral density $G^T(f)$ shown in Fig. 1(a), fourier amplitudes $A^T[k]$ is calculated by $G^T(f_k)$ using Eq. (2) and is shown in Fig. 1(b); and the kth realizations of a uniformly distributed random phase angles $\phi_1[k]$ from $-\pi$ to π shown in Fig. 1(c) are generated for the simulation of Gaussian signal. Then a sample sequence $x_1[n]$ of Gaussian stochastic processes shown in Fig. 1(d) is simulated by Inverse Fast Fourier Transform of $A^T[k]$ and $\phi_1[k]$. The $G^T(f)$ is a flat broadband spectrum with a bandwidth of 1980 Hz (20~2000 Hz), and the spectrum magnitude is 0.02g²/ Hz. The total RMS value σ of acceleration is about 6.29Grms. According to the sampling theorem, some simulation parameters are set as $f_s = 5120Hz$, $M = 4096$, $\Delta f = 1.25Hz$. These three parameters will keep the same during the following simulation experiments.

In order to generate a symmetric super-Gaussian random signal with the same spectrum $G^T(f)$ and target kurtosis value K^T of 4.0, it is a key issue that how to use the non-Gaussian features (skewness and kurtosis) of the stochastic processes to be simulated to reconstruct the phases ϕ_k in Eq. (1) or Eq. (10) for the subsequent IFFT in Eq. (9). To date several phase reconstruction methods have been developed. However, most these methods are very complicated, not sufficiently intuitive, requiring repeated iteration, or with the low simulation accuracy and efficiency. As the main difference in time history between non-Gaussian and Gaussian stochastic processes exists in the Amplitude Probability Density Function (APDF), it can be feasible to approximate the required non-Gaussian features directly through the amplitude modulation of Gaussian stochastic processes, then the reconstructed phases corresponding to non-Gaussian features can be extracted using FFT accurately and quickly. The above idea can be illustrated by Figs. 2 and 3.

(a) Time history of Gaussian signal   (b) Time history of super-Gaussian signal
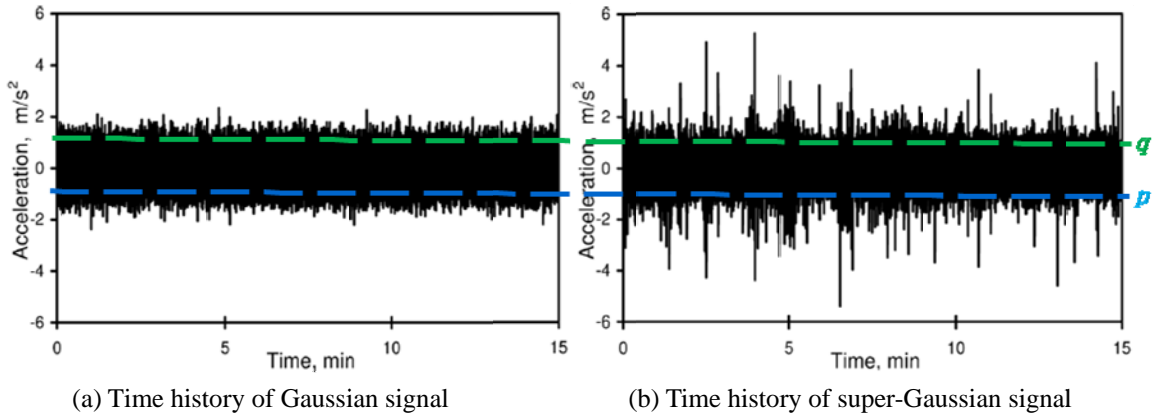
Fig. 2 The difference in time history between super -Gaussian and Gaussian signal
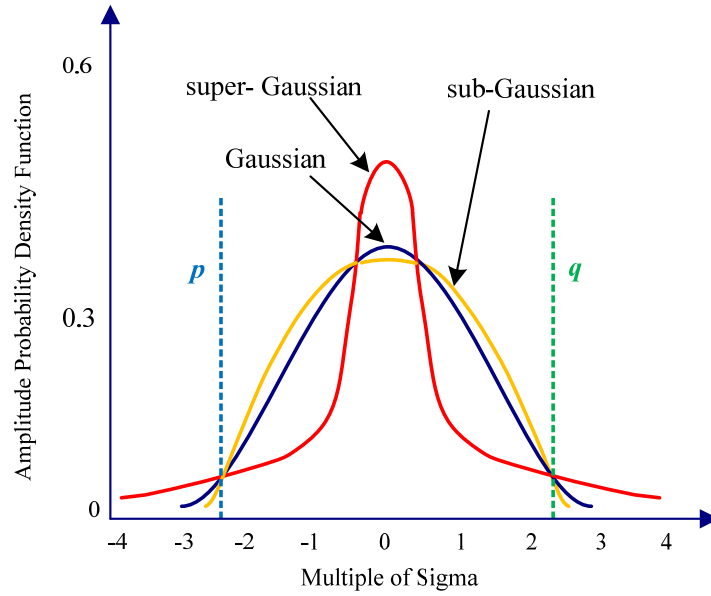
Fig. 3 The difference in APDF between non-Gaussian and Gaussian signal

According to the distributions of Probability Density Function (PDF) of Gaussian and non-Gaussian amplitude sequences in Fig. 3, it can be observed that the main difference between the two PDFs lies in the different tail distributions i.e. in the regions on both sides (less than p or greater than q), super-Gaussian random process has a more significant amplitude distribution than normal Gaussian process. Similarly, Gaussian random process also has a more significant amplitude distribution than sub-Gaussian process in these regions. Thus, in order to artificially generate super-Gaussian signal, we can 'move' some parts of the Gaussian PDF within the region between the two reference values p and q to the outer regions on both sides (less than p or greater than q) according to the axis of symmetry at p and q respectively. This is shown in Eq. (15). Conversely, in order to generate sub-Gaussian signal, we can 'move' some parts in the outer regions (less than p or greater than q) of Gaussian amplitude distribution to the inner region (greater than p and less than q) according to the axis of symmetry at p and q respectively. It is also shown in Eq. (16). Then the required non-Gaussian phases can be obtained through Fourier transform of the acquired non-Gaussian signal.

Then according to Eq. (15), the modification of amplitude distribution from Gaussian sequence $x_1[n]$ to super-Gaussian sequence $x_2[n]$ in the time domain can be implemented.

$$x_2[n] = \begin{cases} 2p - x_1[n] & if \quad p < x_1[n] < 0 \\ 2q - x_1[n] & if \quad 0 < x_1[n] < q \end{cases} \tag{15}$$

Where $p = -\alpha \times \sigma, q = \beta \times \sigma$. And σ is root mean square value (RMS) of Gaussian sequence $x_1[n]$. Specifically, α and β are the parameters which control the size of interval for the amplitude modulation. And these two parameters also control the number of the modulated amplitudes together with some other parameters. Compared with the Gaussian stochastic processes whose most amplitudes (99.74%) are located within the range from -3σ to 3σ on the horizontal axis of APDF, the super-Gaussian stochastic processes has a much wider tail distribution which means more amplitudes outside the range, while the sub-Gaussian stochastic processes has a much narrower tail distribution which demonstrates more amplitudes inside the range. Therefore, these two parameters can be generally set in the range $1 \le \alpha, \beta \le 3$. Moreover, according to Eq. (15), the larger the kurtosis value of a super-Gaussian sequence is, the closer the values of α and β should be selected to 3. In this way, there will be a larger number of adjustable amplitudes, and will help to increase the kurtosis value of the sequence more after amplitude modulation.

Similarly, Eq. (16) is the special amplitude modulation formula for sub-Gaussian sequence.

$$x_2[n] = \begin{cases} 2p - x_1[n] & if \quad x_1[n] < p \\ 2q - x_1[n] & if \quad x_1[n] > q \end{cases} \tag{16}$$

Taking Eq. (16) into consideration, the smaller the kurtosis value of a sub-Gaussian sequence is, the farther the values of α and β should be selected from 3. On the basis of this, there will be a larger number of adjustable amplitudes, and will decrease the kurtosis value of the sequence more after amplitude modulation.

Further, whether the same value is selected to α and β determines that the adjusted amplitude distribution is symmetric or not. Thus it plays a role in determining the value of skewness. That is to say, if $\alpha = \beta$, a non-Gaussian random sequence with the symmetric amplitude distribution will be generated; If $\alpha > \beta$, the amplitude distribution will shift toward the negative direction of the horizontal axis of APDF and skewness value will become negative; Whereas, if $\alpha < \beta$, the amplitude distribution will shift toward the positive direction of the horizontal axis of APDF and the skewness value will become positive.
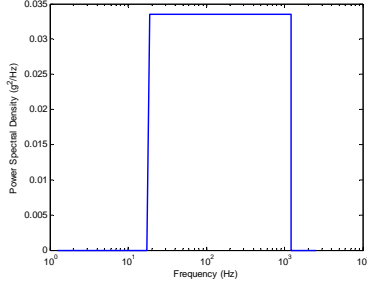
Now we use the above idea to modulate the amplitudes of Gaussian signal $x_1[n]$ step by step in the time domain according to the target kurtosis value K^T of 4.0. Fig. 1(e) shows the modulated signal $x_2[n]$ obtained by amplitude modulation of the original Gaussian signal $x_1[n]$ using Eq. (15). Apparently $x_2[n]$ has a distinctive super-Gaussian feature. The kurtosis value of $x_2[n]$ is about 3.98, while the PSD of $x_2[n]$ shown in Fig. 1(f) deviates from the target PSD $G^T(f)$ because of the amplitude modulation. But it does not matter since the main purpose of amplitude modulation is to get the phase angles corresponding to non-Gaussian features. Fig. 1(g) shows the reconstructed phase angles $\phi_2[k]$ obtained by FFT of the modulated signal $x_2[n]$. Then the fourier amplitudes $A^T[k]$ and the phases angles $\phi_2[k]$ are combined in the subsequent Inverse Fast Fourier Transform (IFFT) to generate the final signal $x_3[n]$. However, despite

having the phase angles of the super-Gaussian signal $x_2[n]$, the time history of $x_3[n]$ shown in Fig. 1(h) has no significant non-Gaussian features. Further, the kurtosis value of $x_3[n]$ is about 0.06, which is very close to the theoretical kurtosis value 0 of Gaussian process. It is obvious that the PSD bandwidth of the modulated signal $x_2[n]$ has a significant effect on the non-Gaussian features of the final signal $x_3[n]$. Further it can be seen that the modulated signal $x_2[n]$ and the original Gaussian signal $x_1[n]$ have the same PSD bandwidth, and the PSD bandwidth has a direct relationship with fourier amplitudes defined by Eq. (2). Therefore simulation experiment 1 shows that non-Gaussian features of the simulated signal by IFFT is not only sensitive to the phase part of IFFT, but also sensitive to the amplitude part of IFFT. This result is very interesting and further inspires us to try to change PSD bandwidth of the original Gaussian signal to obtain the required non-Gaussian signal, since the PSD bandwidth has a direct effect on the amplitude part. Simulation experiment 2 is designed to investigate the effects of the PSD bandwidth of the original Gaussian signal on the final non-Gaussian features.
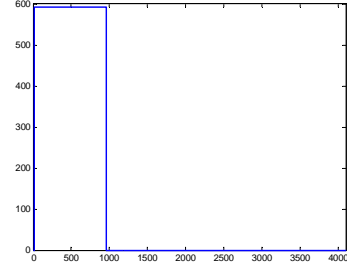
The idea is to change the bandwidth of the original Gaussian signal $x_4[n]$ by the bandwidth coefficient γ. The value of γ is in the range between 0 and 1. Here we set $\gamma = 3/5$ as an example, which means that the PSD bandwidth of $x_4[n]$ is equal to 3/5 of the target PSD bandwidth. In order to maintain the same RMS value of 6.29Grms, the target PSD magnitude of $x_4[n]$ is adjusted to 0.0335g^2/ Hz. Fig. 4(a) shows the modified target PSD $G_1^T(f)$ of $x_4[n]$, and Fig. 4(b) shows the fourier amplitudes $A_1^T[k]$ of $x_4[n]$ calculated by $G_1^T(f_k)$ using Eq.(2). The kth realizations of uniformly distributed random phase angles $\phi_4[k]$ from $-\pi$ to π shown in Fig. 4(c) are generated for the simulation of Gaussian signal $x_4[n]$. Then a sample sequence $x_4[n]$ of Gaussian stochastic processes shown in Fig. 4(d) is simulated by Inverse Fast Fourier Transform of $A_1^T[k]$ and $\phi_4[k]$. Fig. 4(e) shows the modulated signal $x_5[n]$ obtained by amplitude modulation of the original Gaussian signal $x_4[n]$ using Eq. (15). The PSD of $x_5[n]$ is shown in Fig. 4(f). Fig. 4(g) shows the reconstructed phase angles $\phi_5[k]$ obtained by FFT of the modulated signal $x_5[n]$. Then the fourier amplitudes $A^T[k]$ corresponding to the target PSD $G^T(f)$ and the phases angles $\phi_5[k]$ are combined in the subsequent Inverse Fast Fourier Transform (IFFT) to generate the final signal $x_6[n]$. It is obvious that the time history of $x_6[n]$ shown in Fig. 4(h) has significant super-Gaussian features. The kurtosis value of $x_6[n]$ is about 4.06, which is very close to the target kurtosis value K^T of 4.0. The PSD of $x_6[n]$ is strictly equal to the target PSD $G^T(f)$ because the fourier amplitudes of $x_6[n]$ is $A^T[k]$.

In summary, simulation experiment 1 and 2 show that the amplitudes and phases of IFFT have a coupling effect on the non-Gaussian features, and the non-Gaussian features of the simulated signal by IFFT is specifically sensitive to the PSD bandwidth. Then we will further develop a new
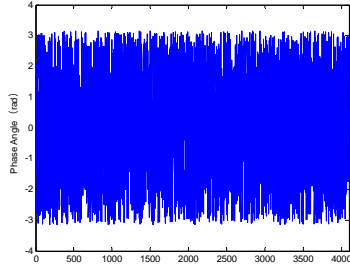
methodology for simulation of various types of non-Gaussian signals by amplitude modulation and phase reconstruction, which will be described as follows.
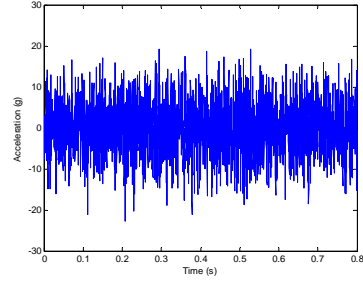

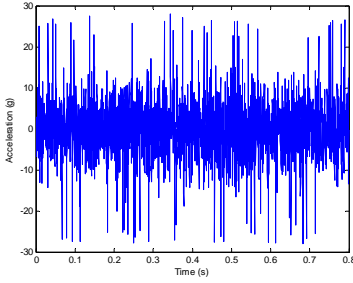(a) Modified target PSD $G_1^T(f)$ of $x_4[n]$
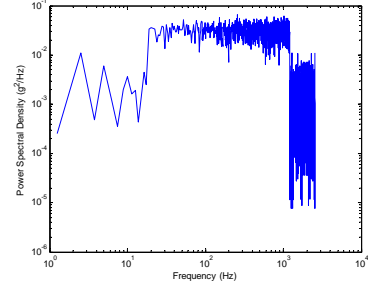
(b) Fourier amplitudes $A_1^T[k]$ of $x_4[n]$

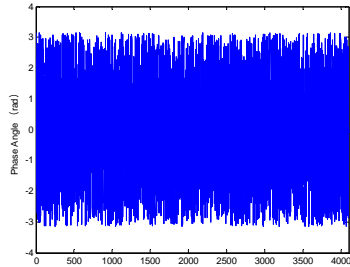(c) Phase angles $\phi_4[k]$ of $x_4[n]$
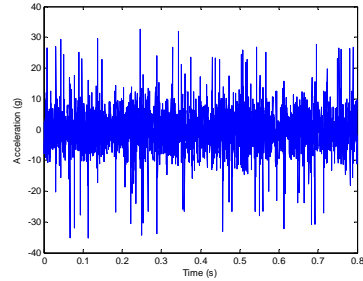
(d) Simulated Gaussian signal $x_4[n]$

(e) Modulated signal $x_5[n]$

(f) PSD of $x_5[n]$

(g) Phase angles $\phi_5[k]$ of $x_5[n]$

(h) Simulated super-Gaussian signal $x_6[n]$

Fig. 4 Simulation experiment 2

4. Simulation algorithm of Non-Gaussian stochastic processes

According to the above simulation results, the new algorithm for simulation of non-Gaussian stochastic processes by amplitude modulation and phase reconstruction is divided into 11 steps shown in Fig. 5.
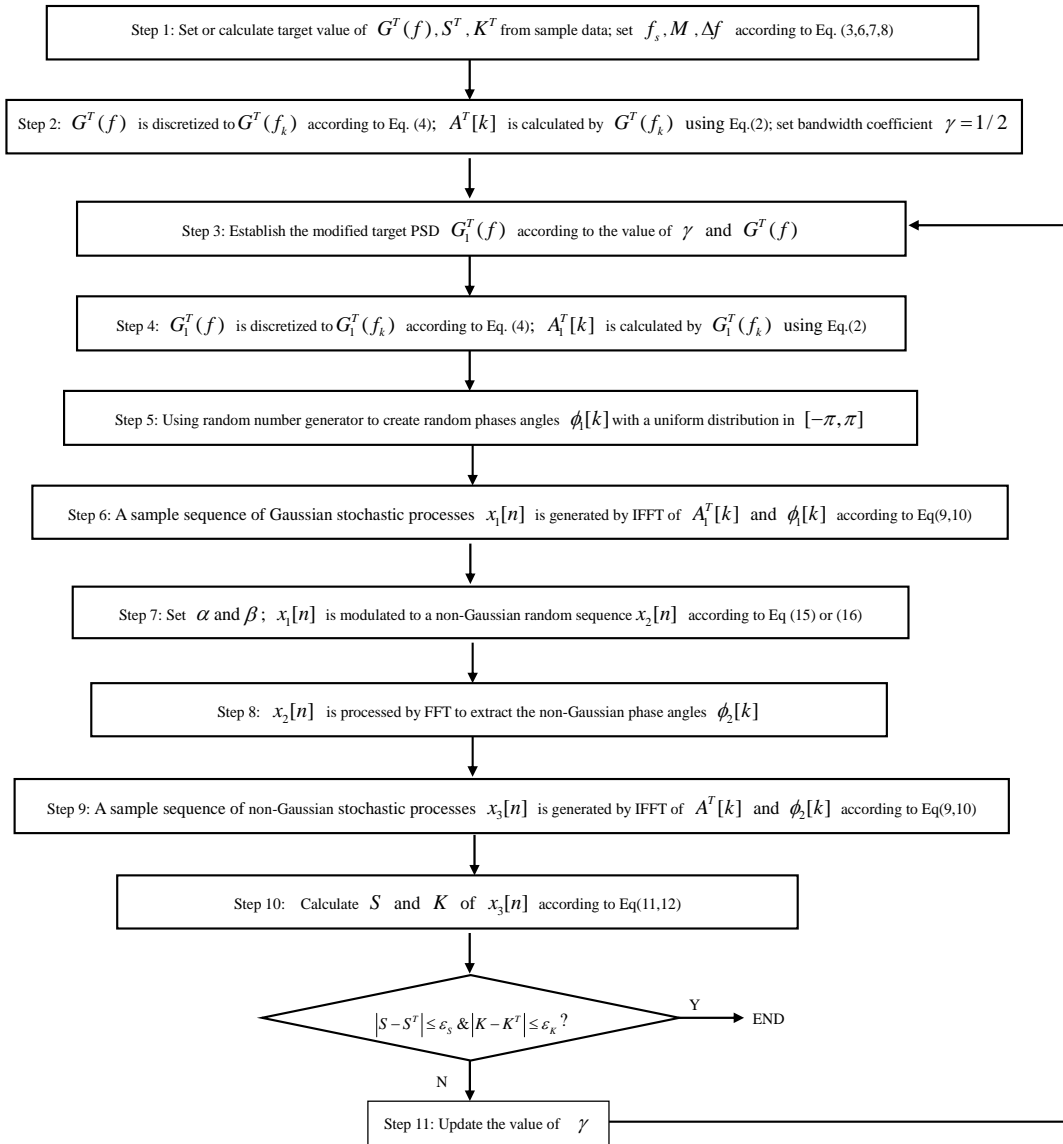
Step 1: Set or calculate target value of $G^T(f)$, S^T, K^T from sample data; set f_s, M, Δf according to Eq. (3,6,7,8)

Step 2: $G^T(f)$ is discretized to $G^T(f_k)$ according to Eq. (4); $A^T[k]$ is calculated by $G^T(f_k)$ using Eq.(2); set bandwidth coefficient $\gamma = 1/2$

Step 3: Establish the modified target PSD $G_1^T(f)$ according to the value of γ and $G^T(f)$

Step 4: $G_1^T(f)$ is discretized to $G_1^T(f_k)$ according to Eq. (4); $A_1^T[k]$ is calculated by $G_1^T(f_k)$ using Eq.(2)

Step 5: Using random number generator to create random phases angles $\phi_1[k]$ with a uniform distribution in $[-\pi, \pi]$

Step 6: A sample sequence of Gaussian stochastic processes $x_1[n]$ is generated by IFFT of $A_1^T[k]$ and $\phi_1[k]$ according to Eq(9,10)

Step 7: Set α and β; $x_1[n]$ is modulated to a non-Gaussian random sequence $x_2[n]$ according to Eq (15) or (16)

Step 8: $x_2[n]$ is processed by FFT to extract the non-Gaussian phase angles $\phi_2[k]$

Step 9: A sample sequence of non-Gaussian stochastic processes $x_3[n]$ is generated by IFFT of $A^T[k]$ and $\phi_2[k]$ according to Eq(9,10)

Step 10: Calculate S and K of $x_3[n]$ according to Eq(11,12)

$|S - S^T| \le \varepsilon_S$ & $|K - K^T| \le \varepsilon_K$? — Y — END

N

Step 11: Update the value of γ

Fig. 5 Simulation algorithm of non-Gaussian stochastic processes

In the simulation process, the initial value of γ can be set to 1/2. Each time after the amplitude modulation and phase reconstruction, skewness S and kurtosis K of the signal simulated by IFFT will be calculated and compared with the target values S^T and K^T. If the errors are larger than the acceptable errors of skewness and kurtosis(ε_S and ε_K), the parameters γ should be updated. So it will be an iteration process before finally reaching the target values. Since this method directly using the amplitude modulation to approximate target non-Gaussian parameters is more clear and concise than other modulation approaches, it is able to approach the target value more quickly, efficiently and accurately. In addition, FFT is generally used to calculate the spectrum, but this algorithm takes advantage of the FFT to extract phase information and the IFFT to generate random signal. This is another feature of the present algorithm.

5. Cases studies

5.1 Case Study 1: Simulation of super-Gaussian truck road vibration record

Fig. 6(a) is a time history of truck body vertical acceleration from road vibration measurements. With the sampling rate of 1280Hz, the time history record was about 12.8 seconds long with 16384 data points. From these measured real-life data, the PSD has been calculated and shown in Fig. 6(b). The skewness and kurtosis coefficients have also been calculated, and the value of S^T and K^T is 0.53 and 12.32 respectively. The total RMS value of acceleration is about 1.48Grms. The APDF of the measured data is shown in Fig. 6(d) by the blue dashed curve, which is significantly different from the red solid curve of standard normal distribution. Fig. 6(c) shows the time history of the simulated vibration data. The APDF of simulated vibration data is shown in Fig. 6(d) by the green dotted curve, which is close to that of the measured dada. Obviously, the amplitude distribution of measured and simulated data are super-Gaussian. The kurtosis value of simulated vibration data is 12.23, which is very close to the target value 12.32. And the skewness value of simulated vibration data is 0.58, which is very close to the target value 0.53. In addition, the PSD of simulated vibration data is strictly equal to that of the measured dada, and the RMS is also equal to 1.48Grms.

5.2 Case study 2: simulation of sub-Gaussian random vibration for structural modal testing

Modal testing is useful to identify resonances and notches in the structural dynamic response. Suppose we need the shaker to provide a broadband random excitation that is typical for modal testing with a uniform PSD shown in Fig. 7(a). The total RMS value of excitation is about 20 Grms.

If we use traditional Gaussian random vibration control mode with a crest factor of 4, the acceleration time history will look something like what is shown in Fig. 7(c) with the maximum peak value somewhere around 80g. The APDF of traditional Gaussian random vibration control signal is shown in Fig. 7(b) by the blue dashed curve, which is close to the red solid curve of standard Gaussian distribution. However，the maximum acceleration limit of the shaker design

capability is 70g. Then it is necessary to generate sub-Gaussian vibration excitation with a lower peak value on the shaker for modal testing. The time history of simulated sub-Gaussian vibration excitation with a decreased kurtosis value of -0.46 is shown in Fig. 7(d). The APDF of simulated sub-Gaussian vibration excitation is shown in Fig. 7(b) by the green dotted curve. The maximum peak value of the sub-Gaussian vibration excitation with the same RMS is about 56 g, which is in the maximum acceleration limit of the shaker design capability. Hence, the sub-Gaussian random vibration control mode can increase the shaker power in structural modal testing.

5.3 Case study 3: design and validation of non-Gaussian random vibration controller

Vibration environment is one of most important environmental factor that may cause structure failure. The simulation of vibration environment in laboratory is very necessary. To further verify the above algorithm, we developed a new non-Gaussian random vibration controller (NRVCS) for electrodynamic or hydraulic shaker. Figs. 8(a) and 8(b) respectively show the hardware and software of non-Gaussian random vibration controller. The actual non-Gaussian vibration testing on the shaker shown in Fig. 8(c) confirmed that NRVCS met the real-time requirement of closed loop vibration control, which validated the efficiency and accuracy of the proposed algorithm.
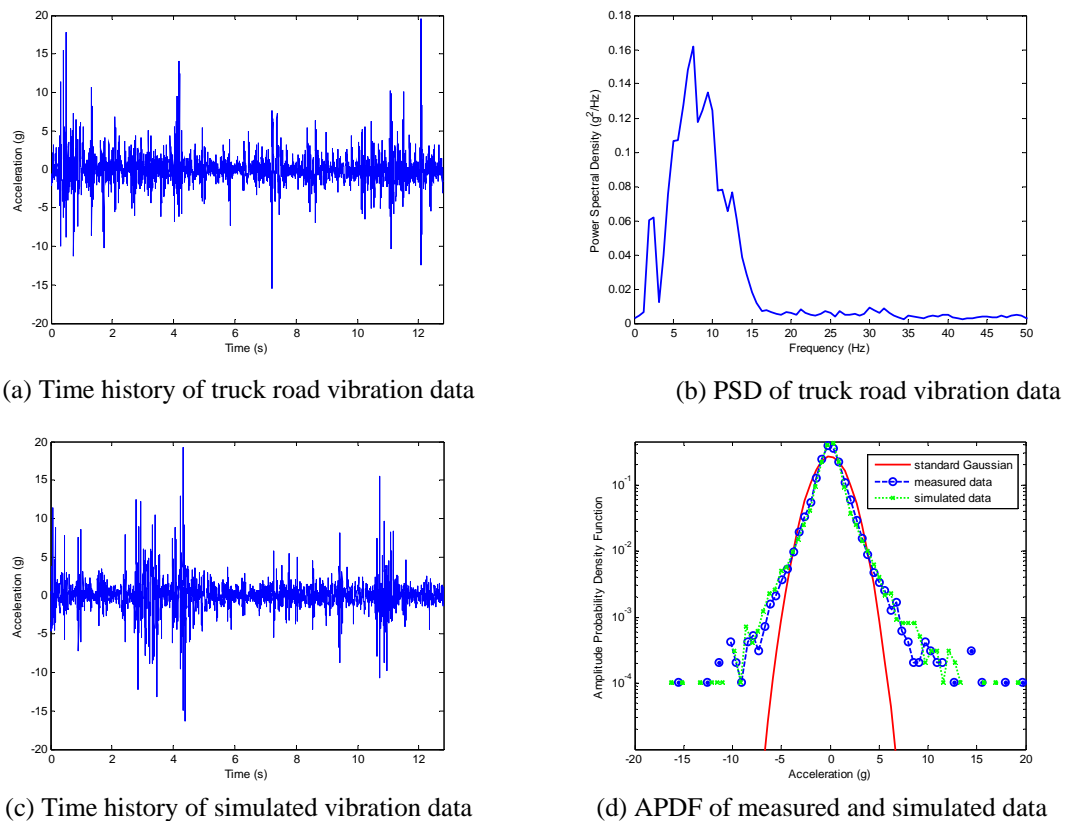

(a) Time history of truck road vibration data

(b) PSD of truck road vibration data

(c) Time history of simulated vibration data

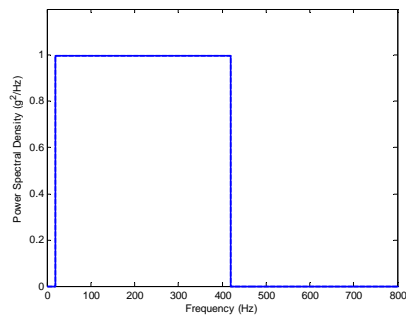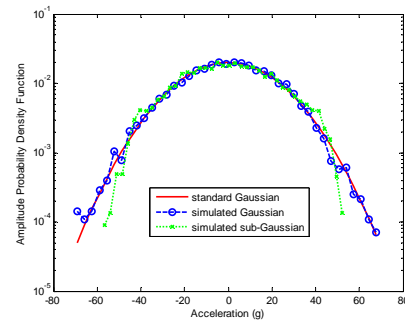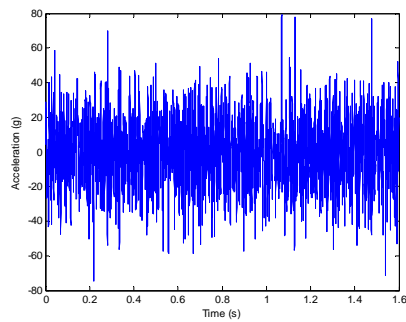(d) APDF of measured and simulated data
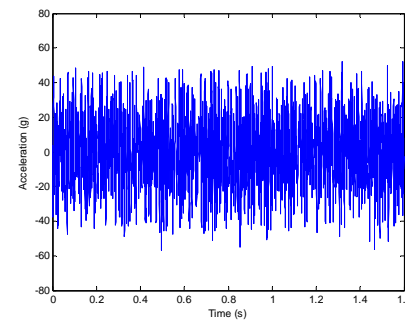
Fig. 6 Case study 1

(a) Target PSD of vibration excitation

(b) APDF of simulated random vibration

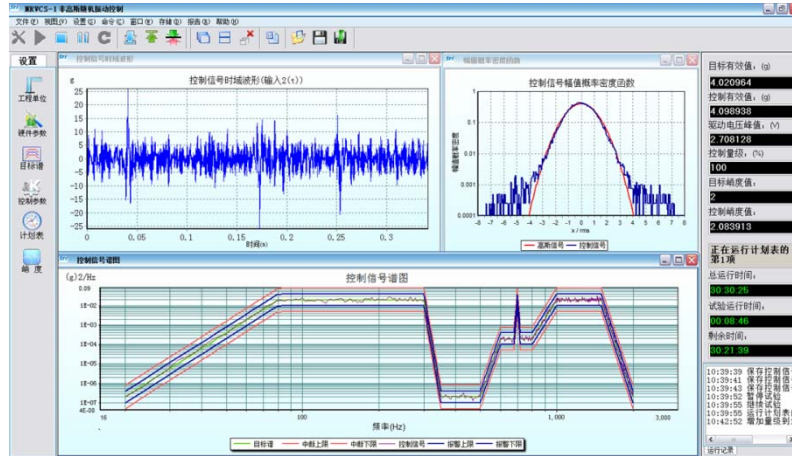(c) Time history of Gaussian random vibration

(d) Time history of sub-Gaussian random vibration

Fig. 7 Case study 2

(a)   Hardware of Non-Gaussian random vibration controller

Continued-

(b) Software of Non-Gaussian random vibration controller

(c) Actual non-Gaussian vibration testing on the shaker

Fig. 8 Case study 3

6. Conclusions

By revealing the inherent coupling effect of the phase and amplitude part of discrete Fourier representation of random time series on the non-Gaussian features (such as skewness and kurtosis) through theoretical analysis and simulation experiments, a novel simulation technique by amplitude modulation and phase reconstruction for non-Gaussian stochastic processes is developed. The major innovation of the proposed methodology is that the desired phase part of the Fourier coefficient for the simulation of non-Gaussian stochastic processes is reconstructed by direct amplitude modulation in the time-domain. As compared to previous spectral representation method using phase modulation to obtain a non-Gaussian amplitude distribution, this non-Gaussian phase reconstruction strategy is more straightforward and efficient. So this method can easily obtain the desired non-Gaussian amplitude distribution characteristics, not only

applicable to the simulation of the super-Gaussian but also the sub-Gaussian random processes, having a wide adaptability. Another goodness of this method is taking full advantage of the fast fourier transform technique to improve the simulation efficiency and accuracy. Cases studies have verified the efficiency and accuracy of this method. The proposed method has a wide range of applicability to engineering problems involving stochastic fields where the Gaussian assumption is not appropriate. This will aid in the modeling and simulating the stochastic dynamic behavior of complex structures to rationally improve their safety and reliability.

Acknowledgements

References

Aung, N.N. and Jihong, Y. (2011), "Simulation of non-Gaussian wind pressure fields on domed structures", *Adv. Mater. Res*., **163-167**, 4142-4148.
Aung, N.N. and Jihong, Y. (2012), "Simulation of multivariate non-Gaussian wind pressure on spherical latticed structures", *Wind Struct.*, **15**(3), 223-245.
Bendat, J.S. and Piersol, A.G. (1986), *Random data: analysis and measurement procedures*, 2nd Ed., New York.
Bocchini, P. and Deodatis, G. (2008), "Critical review and latest developments of a class of simulation algorithms for strongly non-Gaussian random fields", *Probab. Eng. Mech.*, **23**(4), 393-407.
Choi, H. and Kanda, J. (2003), "Translation method: A historical review and its application to simulation of non-Gaussian stationary processes", *Wind Struct.*, **6**(5), 357-386.
Gioffrè, M., Gusella, V. and Grigoriu, M. (2000), "Simulation of non-Gaussian field applied to wind pressure fluctuations", *Probab. Eng. Mech.*, **15**(4), 339-345.
Gurley, K.R., Kareem, A. and Tognarelli, M.A. (1996), "Simulation of a class of non-normal random processes", *Int. J. Nonlinear Mech.*, **31**(5), 601-617.
Li, J. and Li, C. (2012), "Simulation of Non-Gaussian stochastic process with target power spectral density and lower-order moments", *J. Eng. Mech.- ASCE*, **138**(5), 391-404.
Li, J. and Wang, X. (2012), "An exponential model for fast simulation of multivariate non-Gaussian processes with application to structural wind engineering", *Probab. Eng. Mech.*, **30**, 37-47.
Luo, J.J., Su, C. and Han, D.J. (2012), "A simulation methodology of the stationary non-Gaussian stochastic wind pressure field", *Zhendong yu Chongji/J. Vib. Shock*, **31**(10), 111-117.
Phoon, K.K. and Huang, H.W. (2005), "Simulation of strongly non-Gaussian processes using Karhunen-Loeve expansion", *Probab. Eng. Mech.*, **20**(2), 188-198.
Poirion, F. and Puig, B. (2010), "Simulation of non-Gaussian multivariate stationary processes", *Int. J. Nonlinear Mech.*, **45**(5), 587-597.
Seong, S.H. and Peterka, J.A (1998), "Digital generation of surface-pressure fluctuations with spiky features", *J. Wind Eng. Ind. Aerod.*, **73**(2), 181-192.
Seong, S.H. and Peterka, J.A. (2001), "Experiments on fourier phases for synthesis of non-Gaussian spikes in turbulence time series", *J. Wind Eng. Ind. Aerod.*, **89**(5), 421-443.
Shields, M.D. and Deodatis, G. (2011), "Simulation of strongly non-Gaussian stochastic vector processes using translation process theory", *Proceedings of the 11th International Conference on Applications of Statistics and Probability in Civil Engineering*.

Shields, M.D. and Deodatis, G. (2013), "A simple and efficient methodology to approximate a general non-Gaussian stationary stochastic vector process by a translation process with applications in wind velocity simulation", *Probab. Eng. Mech.*, **31**, 19-29.

Steinwolf, A. (1996), "Approximation and simulation of probability distributions with a variable kurtosis value", *Comput. Stat. Data An.*, **21**(2), 163-180.

Steinwolf, A. (2010), "Shaker random testing with low kurtosis: Review of the methods and application for sigma limiting", *Shock Vib.*, **17**(3), 219-231.

Steinwolf, A. (2007), "Forget clipping: Go random with non-Gaussian sigma limiting and double the shaker power!", *Test Eng. Management*, **69**(3), 10-13.

Suresh Kumar, K. and Stathopoulos, T. (1999), "Synthesis of non-Gaussian wind pressure time series on low building roofs", *Eng. Struct.*, **21**(12), 1086-1100.

Vargas-Guzmán, J.A. (2012), "A Heavy tailed probability distributions for non-Gaussian simulations with higher-order cumulant parameters predicted from sample data", *Stoch. Env. Res. Risk A.*, **26**(6), 765-776.

Yamazaki, F. and Shinozuka, M. (1988), "Digital generation of non-Gaussian stochastic fields", *J. Eng. Mech. - ASCE*, **114**(7),1183-1197.

Ye, J., Ding, J. and Liu, C. (2012), "Numerical simulation of non-Gaussian wind load", *Science China Technol. Sciences*, **55**(11), 3057-3069.

Yu J., Zhang, C. and Chen, X. (2008), "Simulation techniques of non-Gaussian random loadings in structural reliability analysis", *Safety, Reliability and Risk Analysis: Theory, Methods and Applications, Proceedings of the Joint ESREL and SRA-Europe Conference*,1663-1670.

Yura, H.T. and Hanson, S.G. (2012), "Digital simulation of two-dimensional random fields with arbitrary power spectra and non-Gaussian probability distribution functions", *Appl. Optics*, **51**(10), 77-83.

Zentner, I., Poirion, F. and Cacciola, P. (2011), "Simulation of seismic ground motion time histories from data using a non Gaussian stochastic model", *Applications of Statistics and Probability in Civil Engineering -Proceedings of the 11th International Conference on Applications of Statistics and Probability in Civil Engineering*, 2474-2479.

CC

Appendix

The nth-order moments of the random process $x(t)$ can be determined by using the basic definition

$$M_n = \lim_{r \to \infty} \frac{1}{r} \int_0^r \{x(t)\}^n \, dt = \frac{1}{T} \int_0^T \{x(t)\}^n \, dt, n = 2, 3, 4 \qquad (1)$$

When the mean value M_1 of $x(t)$ is zero, the kurtosis and skewness expression of $x(t)$ can be calculated on a basis of the first four moments

$$K = \frac{M_4}{(M_2)^2} - 3 \qquad (2)$$

$$S = \frac{M_3}{(M_2)^{3/2}} \qquad (3)$$

The variance M_2 of $x(t)$ is given by Bendat (1986)

$$M_2 = \frac{1}{2} \sum_{k=0}^{N-1} (a_k{}^2 + b_k{}^2) \qquad (4)$$

The fourth moment M_4 of $x(t)$ can be given by the similar expression

$$M_4 = \frac{1}{T} \int_0^T \left[\sum_{k=0}^{N-1} (a_k \cos 2\pi k \Delta ft + b_k \sin 2\pi k \Delta ft) \right]^4 dt \qquad (5)$$

In formulae (4) and (5), instead of the Fourier amplitudes A_k and phase angles ϕ_k, the cosine a_k and sine b_k harmonic components are represented as

$$a_k = A_k \cos \phi_k, \quad b_k = -A_k \sin \phi_k \qquad (6)$$

Integral (5) has been taken in closed analytical form and the formula for kurtosis has been obtained by Steinwolf (1996)

$$K = \left\{ \sum_{k=0}^{N-1} (a_k^2 + b_k^2) \right\}^{-2} \left\{ -\frac{3}{2} \sum_{k=0}^{N-1} \left[(a_k^2 + b_k^2)^2 \right] + 2 \sum_{j=3k} \left[a_j a_k (a_k^2 - 3b_k^2) - b_j b_k (b_k^2 - 3a_k^2) \right] + \right.$$

$$6 \sum_{\substack{j=k+2n \\ k \neq n}} \left[(a_j a_k + b_j b_k)(a_n^2 - b_n^2) - 2(a_j b_k - a_k b_j) a_n b_n \right] +$$

$$6 \sum_{\substack{j+k=2n \\ j<k}} \left[(a_j a_k - b_j b_k)(a_n^2 - b_n^2) + 2(a_j b_k + a_k b_j) a_n b_n \right] +$$

$$12 \sum_{\substack{j+k=n+m \\ j<k,n<m,j<n}} \left[(a_j a_k - b_j b_k)(a_n a_m - b_n b_m) + (a_j b_k + a_k b_j)(a_n b_m + a_m b_n) \right] +$$

$$\left. 12 \sum_{\substack{j+k+n=m \\ j<k<n}} \left[(a_j a_k - b_j b_k)(a_n a_m + b_n b_m) + (a_j b_k + a_k b_j)(a_n b_m - a_m b_n) \right] \right\}$$

(7)

To further visually see the relationship between the variables in fourier series model and kurtosis, inserting Eq. (6) back into Eq. (7) and applying trigonometric formulas yields

$$\sum_{k=0}^{N-1} (a_k^2 + b_k^2) = \sum_{k=0}^{N-1} A_k^2 \tag{8}$$

$$\sum_{k=0}^{N-1} \left[(a_k^2 + b_k^2)^2 \right] = \sum_{k=0}^{N-1} A_k^4 \tag{9}$$

$$\sum_{j=3k} \left[a_j a_k (a_k^2 - 3b_k^2) - b_j b_k (b_k^2 - 3a_k^2) \right]$$

$$= \sum_{j=3k} \left[(a_j a_k^3 - b_j b_k^3) + 3(b_j b_k a_k^2 - a_j a_k b_k^2) \right]$$

$$= \sum_{j=3k} \left\{ A_j A_k^3 \left[\cos\phi_j \cos\phi_k \cos^2\phi_k - \sin\phi_j \sin\phi_k \sin^2\phi_k \right] + \right.$$

$$\left. 3 A_j A_k^3 \left[\sin\phi_j \sin\phi_k \cos^2\phi_k - \cos\phi_j \cos\phi_k \sin^2\phi_k \right] \right\}$$

$$= \sum_{j=3k} A_j A_k^3 \left[\cos\phi_j \cos\phi_k (\cos^2\phi_k - 3\sin^2\phi_k) + \sin\phi_j \sin\phi_k (3\cos^2\phi_k - \sin^2\phi_k) \right]$$

$$= \sum_{j=3k} A_j A_k^3 \left[\cos\phi_j \cos\phi_k (1 - 4\sin^2\phi_k) + \sin\phi_j \sin\phi_k (4\cos^2\phi_k - 1) \right]$$

$$= \sum_{j=3k} A_j A_k^3 \left[\cos\phi_j \cos\phi_k (2\cos 2\phi_k - 1) + \sin\phi_j \sin\phi_k (2\cos 2\phi_k + 1) \right]$$

$$= \sum_{j=3k} A_j A_k^3 \left[2\cos 2\phi_k (\cos\phi_j \cos\phi_k + \sin\phi_j \sin\phi_k) - (\cos\phi_j \cos\phi_k - \sin\phi_j \sin\phi_k) \right]$$

$$= \sum_{j=3k} A_j A_k^3 \left[2\cos 2\phi_k \cos(\phi_j - \phi_k) - \cos(\phi_j + \phi_k) \right]$$

$$= \sum_{j=3k} A_j A_k^3 \left[2\cos 2\phi_k \cos(\phi_j - \phi_k) - \cos(2\phi_k + \phi_j - \phi_k) \right]$$

$$= \sum_{j=3k} A_j A_k{}^3 \left[2\cos 2\phi_k \cos(\phi_j - \phi_k) - \cos 2\phi_k \cos(\phi_j - \phi_k) + \sin 2\phi_k \sin(\phi_j - \phi_k) \right]$$

$$= \sum_{j=3k} A_j A_k{}^3 \left[\cos 2\phi_k \cos(\phi_j - \phi_k) + \sin 2\phi_k \sin(\phi_j - \phi_k) \right]$$

$$= \sum_{j=3k} A_j A_k{}^3 \cos(\phi_j - 3\phi_k)$$

(10)

$$\sum_{\substack{j=k+2n \\ k \neq n}} \left[(a_j a_k + b_j b_k)(a_n{}^2 - b_n{}^2) - 2(a_j b_k - a_k b_j)a_n b_n \right]$$

$$= \sum_{\substack{j=k+2n \\ k \neq n}} \left[(A_j A_k \cos\phi_j \cos\phi_k + A_j A_k \sin\phi_j \cos\phi_k)(A_n{}^2 \cos^2\phi_n - A_n{}^2 \sin^2\phi_n) \right.$$

$$\left. -2(-A_j A_k \cos\phi_j \sin\phi_k + A_j A_k \sin\phi_j \cos\phi_k)(-A_n{}^2 \sin\phi_n \cos\phi_n) \right]$$

$$= \sum_{\substack{j=k+2n \\ k \neq n}} \left[A_j A_k A_n{}^2 \cos(\phi_j - \phi_k)(\cos^2\phi_n - \sin^2\phi_n) + 2 A_j A_k A_n{}^2 \sin(\phi_j - \phi_k)\sin\phi_n \cos\phi_n) \right]$$

$$= \sum_{\substack{j=k+2n \\ k \neq n}} A_j A_k A_n{}^2 \left[\cos(\phi_j - \phi_k)(2\cos^2\phi_n - 1) + \sin(\phi_j - \phi_k)\sin 2\phi_n \right]$$

$$= \sum_{\substack{j=k+2n \\ k \neq n}} A_j A_k A_n{}^2 \left[\cos(\phi_j - \phi_k)\cos 2\phi_n + \sin(\phi_j - \phi_k)\sin 2\phi_n \right]$$

$$= \sum_{\substack{j=k+2n \\ k \neq n}} A_j A_k A_n{}^2 \cos(\phi_j - \phi_k - 2\phi_n)$$

(11)

$$\sum_{\substack{j+k=2n \\ j<k}} \left[(a_j a_k - b_j b_k)(a_n{}^2 - b_n{}^2) + 2(a_j b_k + a_k b_j)a_n b_n \right]$$

$$= \sum_{\substack{j+k=2n \\ j<k}} \left[(A_j A_k \cos\phi_j \cos\phi_k - A_j A_k \sin\phi_j \cos\phi_k)(A_n{}^2 \cos^2\phi_n - A_n{}^2 \sin^2\phi_n) \right.$$

$$\left. +2(-A_j A_k \cos\phi_j \sin\phi_k - A_j A_k \sin\phi_j \cos\phi_k)(-A_n{}^2 \sin\phi_n \cos\phi_n) \right]$$

$$= \sum_{\substack{j+k=2n \\ j<k}} \left[A_j A_k A_n{}^2 \cos(\phi_j + \phi_k)(\cos^2\phi_n - \sin^2\phi_n) + 2 A_j A_k A_n{}^2 \sin(\phi_j + \phi_k)\sin\phi_n \cos\phi_n) \right]$$

$$= \sum_{\substack{j+k=2n \\ j<k}} A_j A_k A_n{}^2 \left[\cos(\phi_j + \phi_k)(2\cos^2\phi_n - 1) + \sin(\phi_j + \phi_k)\sin 2\phi_n \right]$$

$$= \sum_{\substack{j+k=2n \\ j<k}} A_j A_k A_n{}^2 \left[\cos(\phi_j + \phi_k)\cos 2\phi_n + \sin(\phi_j + \phi_k)\sin 2\phi_n \right]$$

$$= \sum_{\substack{j+k=2n \\ j<k}} A_j A_k A_n{}^2 \cos(\phi_j + \phi_k - 2\phi_n)$$

(12)

$$\sum_{\substack{j+k=n+m \\ j<k,n<m,j<n}} \left[(a_j a_k - b_j b_k)(a_n a_m - b_n b_m) + (a_j b_k + a_k b_j)(a_n b_m + a_m b_n) \right]$$

$$= \sum_{\substack{j+k=n+m \\ j<k,n<m,j<n}} \left[(A_j A_k \cos\phi_j \cos\phi_k - A_j A_k \sin\phi_j \sin\phi_k)(A_n A_m \cos\phi_n \cos\phi_m - A_n A_m \sin\phi_n \sin\phi_m) + \right.$$

$$\left. (-A_j A_k \cos\phi_j \sin\phi_k - A_j A_k \sin\phi_j \cos\phi_k)(-A_n A_m \cos\phi_n \sin\phi_m - A_n A_m \sin\phi_n \cos\phi_m) \right]$$

$$= \sum_{\substack{j+k=n+m \\ j<k,n<m,j<n}} \left[A_j A_k A_n A_m \cos(\phi_j + \phi_k)\cos(\phi_n + \phi_m) + A_j A_k A_n A_m \sin(\phi_j + \phi_k)\sin(\phi_n + \phi_m) \right]$$

$$= \sum_{\substack{j+k=n+m \\ j<k,n<m,j<n}} A_j A_k A_n A_m \cos(\phi_j + \phi_k - \phi_n - \phi_m)$$

$$(13)$$

$$\sum_{\substack{j+k+n=m \\ j<k<n}} \left[(a_j a_k - b_j b_k)(a_n a_m + b_n b_m) + (a_j b_k + a_k b_j)(a_n b_m - a_m b_n) \right]$$

$$= \sum_{\substack{j+k+n=m \\ j<k<n}} \left[(A_j A_k \cos\phi_j \cos\phi_k - A_j A_k \sin\phi_j \sin\phi_k)(A_n A_m \cos\phi_n \cos\phi_m + A_n A_m \sin\phi_n \sin\phi_m) + \right.$$

$$\left. (-A_j A_k \cos\phi_j \sin\phi_k - A_j A_k \sin\phi_j \cos\phi_k)(-A_n A_m \cos\phi_n \sin\phi_m + A_n A_m \sin\phi_n \cos\phi_m) \right]$$

$$= \sum_{\substack{j+k+n=m \\ j<k<n}} \left[A_j A_k A_n A_m \cos(\phi_j + \phi_k)\cos(\phi_m - \phi_n) + A_j A_k A_n A_m \sin(\phi_j + \phi_k)\sin(\phi_m - \phi_n) \right]$$

$$= \sum_{\substack{j+k+n=m \\ j<k<n}} A_j A_k A_n A_m \cos(\phi_j + \phi_k + \phi_n - \phi_m)$$

$$(14)$$

Then the Eq. (7) for kurtosis can be rewritten as

$$K = \left\{ \sum_{k=0}^{N-1} A_k^2 \right\}^{-2} \left\{ -\frac{3}{2} \sum_{k=0}^{N-1} A_k^4 + 2 \sum_{j=3k} A_j A_k^3 \cos(\phi_j - 3\phi_k) + 6 \sum_{\substack{j=k+2n \\ k\neq n}} A_j A_k A_n^2 \cos(\phi_j - \phi_k - 2\phi_n) + \right.$$

$$6 \sum_{\substack{j+k=2n \\ j<k}} A_j A_k A_n^2 \cos(\phi_j + \phi_k - 2\phi_n) + 12 \sum_{\substack{j+k=n+m \\ j<k,n<m,j<n}} A_j A_k A_n A_m \cos(\phi_j + \phi_k - \phi_n - \phi_m) +$$

$$\left. 12 \sum_{\substack{j+k+n=m \\ j<k<n}} A_j A_k A_n A_m \cos(\phi_j + \phi_k + \phi_n - \phi_m) \right\}$$

$$(15)$$